SCIENCE CHINA
Chemistry

•REVIEWS•
SPECIAL ISSUE: 2020 Emerging Investigator Issue

October 2020 Vol.63 No.10: 1416–1427
https://doi.org/10.1007/s11426-020-9767-9

Efficient photocatalysis triggered by thin carbon layers coating on photocatalysts: recent progress and future perspectives

Yu-Long Men, Peng Liu, Xingcui Peng & Yun-Xiang Pan*

Institute of Nano Biomedicine and Engineering, Shanghai Engineering Research Centre for Intelligent Diagnosis and Treatment Instrument, Department of Instrument Science and Engineering, School of Electronic Information and Electrical Engineering, Shanghai Jiao Tong University, Shanghai 200240, China

Received March 30, 2020; accepted May 6, 2020; published online May 19, 2020

Solar-energy-driven photocatalysis, such as photocatalytic reduction of CO_2, is promising simultaneously for the energy and environmental issues. Coating thin carbon layers with the thickness less than 10 nm on photocatalysts has been developed as an efficient strategy for enhancing the photocatalytic efficiency in recent years. In the present review, we summarize the crucial progress on carbon-coated photocatalysts. Origins for the improved light absorption, charge separation, reactant adsorption and photocatalytic stability on carbon-coated photocatalysts as well as the applications of carbon-coated photocatalysts are discussed. Future opportunities and challenges associated with carbon-coated photocatalysts are shown at the end of the review. We hope that the present review can trigger more deep insights on carbon-coated photocatalysts and provide new opportunities for developing low-cost but efficient photocatalysts.

carbon-coated photocatalysts, light absorption, charge separation, reactant adsorption, photocatalytic stability

Citation: Men YL, Liu P, Peng X, Pan YX. Efficient photocatalysis triggered by thin carbon layers coating on photocatalysts: recent progress and future perspectives. *Sci China Chem*, 2020, 63: 1416–1427, https://doi.org/10.1007/s11426-020-9767-9

1 Introduction

Energy crisis and environmental pollution have become the most serious concerns for the mankinds [1]. Solar-energy-driven photocatalysis is a promising strategy to simultaneously solve the energy and environmental issues [1–10]. For example, the photocatalytic reduction of carbon dioxide (CO_2) can not only alleviate CO_2 emission, but also produce valuable chemicals like methanol (CH_3OH) [5–7]. Generally, a photocatalytic reaction proceeds *via* five steps, including (i) light absorption by photocatalysts to generate electron-hole pairs, (ii) separation of the electron-hole pairs, (iii) transfer of the electrons and holes independently, (iv) adsorption of reactants on photocatalysts and (v) reaction of the adsorbed reactants with the photogenerated charge carriers [6–10]. Ideal photocatalysts should have high efficiencies in all of the above steps. But, most of the developed photocatalysts suffer from inferior light absorption, fast electron-hole recombination, poor reactant adsorption and low stability [4–14]. This makes the photocatalytic efficiency still far below the requirement of large-scale commercialization.

Carbon, one of the most abundant elements on earth, has attracted great attention in photocatalysis [14–24]. The carbon atom is an excellent dopant for photocatalysts, *e.g.*, TiO_2. The carbon dopant enters into photocatalyst lattices, as a substitutional anion or/and an interstitial cation, creating mid-gap states in the band gaps of photocatalysts. This favors for extending light absorption, separating photogenerated electron-hole pairs and adsorbing reactants on photocatalysts, thus

*Corresponding author (email: yxpan81@sjtu.edu.cn)

improving the photocatalytic efficiency [15–19]. Carbon-based materials, *e.g.*, graphene, are excellent supports for photocatalysts, *e.g.*, CdS, due to their tunable structural properties, unique surface chemistry, superior electronic conductivity as well as high thermal and chemical stability [20–24]. Photocatalysts are anchored on the carbon-based supports *via* the interactions of photocatalysts with functional groups of the carbon-based supports or/and *via* the bonds between atoms of photocatalysts and carbon atoms of the carbon-based supports. This can efficiently suppress photocatalyst aggregations, thus enlarging surface area and leading to more catalytic active sites for reactions [21,22]. The carbon-based supports can enhance the separation and transfer of the photogenerated charge carriers, resulting in more charge carriers for reactions. These advantages of carbon-based supports facilitate surface reactions, thus increasing photocatalytic efficiency [23,24]. Besides, noble metals, *e.g.*, Pt, are usually used as co-catalysts for providing active sites for photocatalytic reactions [25–27]. But, the low abundance and the high price limit the applications of noble metal co-catalysts in large-scale commercialization. It has been shown that carbon-based materials are excellent alternatives to noble metals, and can be directly used as co-catalysts for photocatalysis [28–34]. For instance, graphene oxide nanosheets were found to be highly efficient co-catalysts for producing CH_3OH from the photocatalytic reduction of CO_2 with H_2O. This is helpful for constructing low-cost but efficient metal-free photocatalysts [34].

Uniformly coating thin carbon layers, graphitic or amorphous, with the thickness less than 10 nm on photocatalysts to enwrap the photocatalysts, is also a very attractive strategy to improve photocatalytic efficiency (Figure 1). The carbon-coating layer can extend light absorption, suppress photocatalyst aggregation, promote charge separation and transfer, and improve reactant adsorption on photocatalysts [35–50]. In addition, different from carbon-based dopants and supports, the carbon layers coating on photocatalysts isolate the photocatalysts from the exterior environment [36,38–41]. This makes the carbon-coating strategy have some unique features. Firstly, the carbon-coated photocatalysts have a high resistance to photocorrosion, heating, acid and alkali [38–43]. Secondly, by changing the porous properties of the carbon coating layer, amounts of photons arriving at photocatalyst surface, photogenerated charge carriers as well as reactant and product molecules transferring between the photocatalysts and the exterior environment can be tuned. This is benefit for increasing the activity and selectivity of photocatalysts [45–50].

Large numbers of reviews about the applications of carbon in photocatalysis have been published. However, these reviews focused on carbon-based dopants and supports, and paid very little attention on carbon-coated photocatalysts [22–24,35,36,51–53]. Due to the unique features, interest in carbon-coated photocatalysts is rapidly increasing. In the present review, we summarize the crucial progress on carbon-coated photocatalysts. Origins for the improved light absorption, charge separation and transfer, reactant adsorption and photocatalytic stability on carbon-coated photocatalysts as well as the applications of carbon-coated photocatalysts are discussed. At the end of the review, we highlight the challenges and opportunities for deep investigations on carbon-coated photocatalysts.

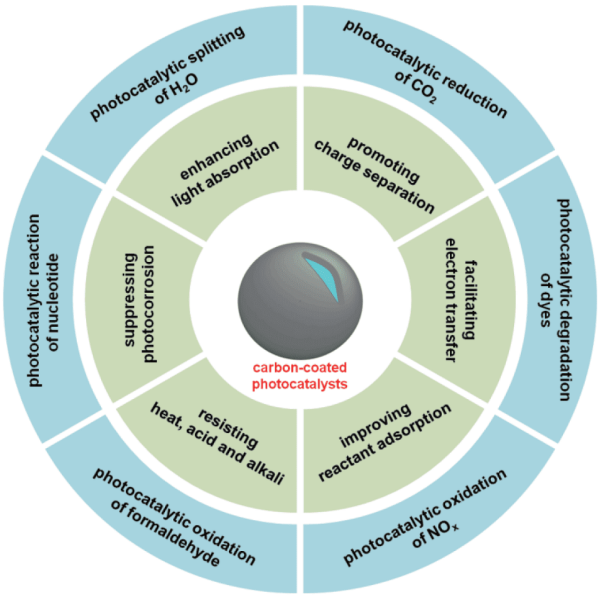

Figure 1 Schematic for the features and applications of carbon-coated photocatalysts (color online).

2 Light absorption

Light absorption by photocatalysts results in the excitation of electrons from the valence band (VB) to the conduction band (CB) on photocatalysts, forming electrons and holes for triggering photocatalytic reactions [11]. Lights in different wavelengths have different energies. The electron excitation from VB to CB can only occur when photocatalysts absorb light with energy larger than their band gaps [54,55]. Ultraviolet light (<400 nm), visible light (400–760 nm) and infrared light (>760 nm) are the main parts of sunlight, and account for about 7%, 50% and 43% of sunlight, respectively. The best scenario that we hope to achieve is that photocatalysts can absorb light in all wavelengths. However, a large number of the developed photocatalysts can only be excited under the irradiation of ultraviolet light due to their wide band gaps, *e.g.*, TiO_2, which is one of the most widely studied photocatalysts [54–56]. Various photocatalysts responsive to visible light, such as CdS and Cu_2O, have also been fabricated, but they usually suffer from high electron-hole recombination rates, low reactant adsorption capacity and poor photocatalytic stability [54–57].

Coating carbon layers on photocatalysts, which are only responsive to ultraviolet light, can extend light absorption to visible regions [37,40,44,50,58–63]. Wang *et al.* [37] coated thin amorphous carbon layers on TiO_2 to form a core-shell C/TiO_2. During the coating process, some carbon atoms entered into the TiO_2 lattice to form some mid-gap states, thus narrowing the band gap of TiO_2 from 3.3 to 2.9 eV. This resulted in an obviously enhanced absorption in visible light on C/TiO_2, as compared with pure TiO_2 without carbon. Zhang *et al.* [40] prepared a series of ZnO@C nanocables through coating ZnO nanowires by carbon layers with the thickness ranging from 3 to 8.5 nm. Pure ZnO without carbon absorbed ultraviolet light only, but ZnO@C exhibited strong absorption in both ultraviolet and visible regions (Figure 2). Sun *et al.* [50] coated In_2O_3 nanoparticles with thin nitrogen-doped carbon layers, and broadened the light absorption of In_2O_3 in 400–800 nm. A composite oxide CuZnO@Fe_3O_4 with a band gap of about 1.90 eV was found to be able to absorb light with wavelengths ranging from 200 to 651 nm. After reduced graphene oxide (rGO) nanosheets with a thickness smaller than 1.0 nm on CuZnO@Fe_3O_4 were coated, the wavelength range of the light absorption was extended to 200–859 nm. The decreased band gap (1.44 eV), which could be caused by the strong interactions between rGO and CuZnO@Fe_3O_4, was suggested to be the origin for the extended light absorption on rGO-coated CuZnO@Fe_3O_4 [58].

Some recent studies showed that, by tuning the structural properties of carbon-coated photocatalysts, the light absorption range can be further extended to infrared regions [64,65]. Liang *et al.* [65] coated thin carbon layers on TiO_2 hierarchical nanotubes (HNTs), nanoparticles (NPs) and nanorods (NRs) to fabricate TiO_2/C HNTs, TiO_2/C NPs and TiO_2/C NRs, respectively. As shown in Figure 3, TiO_2/C HNTs, TiO_2/C NPs and TiO_2/C NRs can absorb the light covering the ultraviolet, visible and infrared regions. The band gaps of TiO_2/C HNTs, TiO_2/ C NPs and TiO_2/C NRs were calculated to be 2.08, 2.37 and 2.26 eV, respectively, which were smaller than that of pristine TiO_2 without carbon (3.3 eV). The smaller band gaps further indicated the enhanced abilities of TiO_2/C HNTs, TiO_2/C NPs and TiO_2/C NRs in light absorption. The light absorption on TiO_2/C HNTs is higher than those of TiO_2/C NPs and TiO_2/C NRs. This could be caused by the hetero multichannel structure formed between TiO_2 HNTs and carbon layers as well as a better light trapping properties and multiple reflectance capability in the hierarchical nanotubes. They also found that the valence band of TiO_2/C HNTs (3.09 eV) located at the site below the potential for H_2O oxidation (1.23 eV). As such, TiO_2/C HNTs was suggested to be benefit for triggering the H_2O oxidation.

The carbon layer in light absorption on carbon-coated photocatalysts has double roles [37,40,50,58–65]. Firstly, the carbon layer is an excellent photosensitizer favoring for

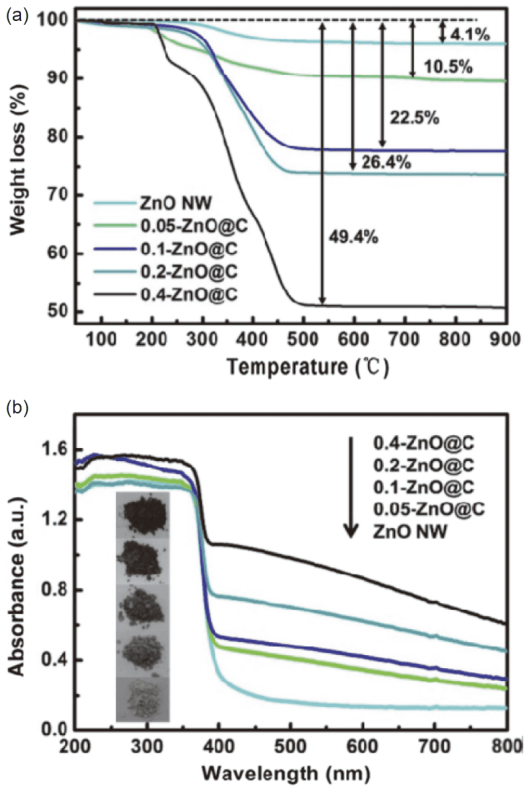

Figure 2 Thermal gravimetric analyses (a) and UV-Vis spectra (b) of ZnO nanowires and ZnO@C nanocables. Insets of (b) are the digital photographs of the materials, adapted with permission from Ref. [40], copyright by Elsevier (2019), and reproduced for clarity (color online).

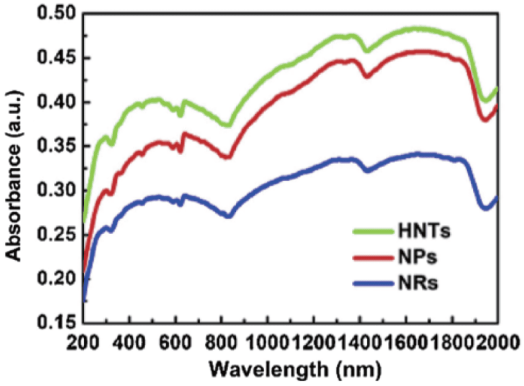

Figure 3 UV-Vis-NIR absorption spectra of TiO_2/C HNTs, TiO_2/C NPs and TiO_2/C NRs, adapted with permission from Ref. [65], copyright by Elsevier (2019) (color online).

enhancing light absorption [59]. Secondly, the strong interaction between carbon layers and photocatalysts leads some carbon atoms to enter into photocatalyst lattices and creates mid-gap states, thus narrowing the band gap of photocatalysts [37,44,59]. This further enhances light absorption. A factor crucial for the light absorption on carbon-coated photocatalysts is the thickness of the carbon layers [40,59,63,65]. Too thick carbon layers prevent the light from

reaching the photocatalyst surface, and plenty of photons are scattered to external environments or/and absorbed by carbon layers [59,65]. This reduces the amount of photons arriving at the photocatalyst surface, and thereby decreases the amount of electrons excited from VB to CB on photocatalysts. When too thin carbon layers are coated on photocatalysts or photocatalysts are not completely coated, there is no obvious extension in light absorption [40,60–65]. Another factor affecting the efficiency of carbon-coated photocatalysts in light absorption is the interaction between carbon layers and photocatalysts [37,61–65]. Some carbon atoms enter into the photocatalyst lattice due to the carbon-photocatalyst interaction with a suitable strength [37]. With too strong carbon-photocatalyst interactions, the conversion of photocatalysts into carbide species, which have poor light absorption capabilities, easily occurs [66]. If the carbon-photocatalyst interaction is too weak, the carbon layer is ineffective in light absorption [61–65]. Thus, a suitable carbon-photocatalyst interaction is essential for enhancing light absorption. In addition, it has been reported that the porous properties of the carbon layer also affected the amount of photons arriving at the photocatalyst surface, and thereby changed the excitation of the electrons from VB to CB on photocatalysts [45–50].

3 Charge separation and transfer

Light absorption by photocatalysts triggers the electron excitation from VB to CB, generating negatively charged electrons on CB and positively charged holes on VB [11]. There are two possible fates for the photogenerated electrons and holes. Firstly, the electrons on CB go back to VB and recombine with the holes. Secondly, the electrons on CB and the holes on VB transfer separately, and then participate in surface reactions [54,55]. Evidently, in order to achieve higher photocatalytic efficiencies, the second fate is highly desired. However, most of the photocatalyts have poor abilities in the charge separation and transfer.

Carbon-coated photocatalysts showed higher efficiencies in separating the photogenerated electron-hole pairs than the photocatalysts without carbon. The carbon layer coating on photocatalysts has low work function and high electron affinity. This makes the carbon layer excellent in capturing the electrons from CB of photocatalysts, and thereby favors for achieving the efficient electron-hole separation. The carbon layer coating on photocatalysts is also an excellent electron transporter, due to its high conductivity. This is benefit for the electron transfer from CB of photocatalysts to the carbon layers, thus promoting the electron-hole separation [45–50,67–80]. Besides, the conductive carbon layer is also flexible for transferring the electrons to catalytic active sites to trigger the surface reactions. For example, Liao *et al.* [67] analyzed the separation of photogenerated electron-hole pairs on carbon-coated ZnO. The work function and the electron affinity of ZnO were 5.4 and 2.088 eV, respectively, while the work function and the electron affinity of the carbon layers located in the ranges of 3.5–4.0 eV and 2.5–3.0 eV, respectively. As illustrated in Figure 4, band bending occurred at the carbon-ZnO interface on carbon-coated ZnO due to the difference in the work functions. This facilitated the flow of electrons from CB of ZnO to the carbon layers. Besides, the higher electron affinity of the carbon layers further promoted the electron transfer from CB of ZnO to the carbon layers. Thus, an enhanced electron-hole separation was achieved on carbon-coated ZnO.

Doping the carbon layer with N atoms, which have electron lone pairs, increases the electron affinity and conductivity of the carbon layer. Thus, photocatalysts coated by N-doped carbon layers exhibit higher efficiencies in separating photogenerated electron-hole pairs, as compared with those coated by pure carbon layers [50,75–77]. Sun *et al.* [50] coated In_2O_3 hollow dodecahedrals (HD) by N-doped carbon layers to form N-C/In_2O_3 HD. Higher cathodic current densities for dissociating H_2O and higher photocurrents (Figure 5(a)) were observed on N-C/In_2O_3 HD, indicating an enhanced ability in the electron transfer on N-C/In_2O_3 HD. In the Nyquist plot from electrochemical impedance spectro-

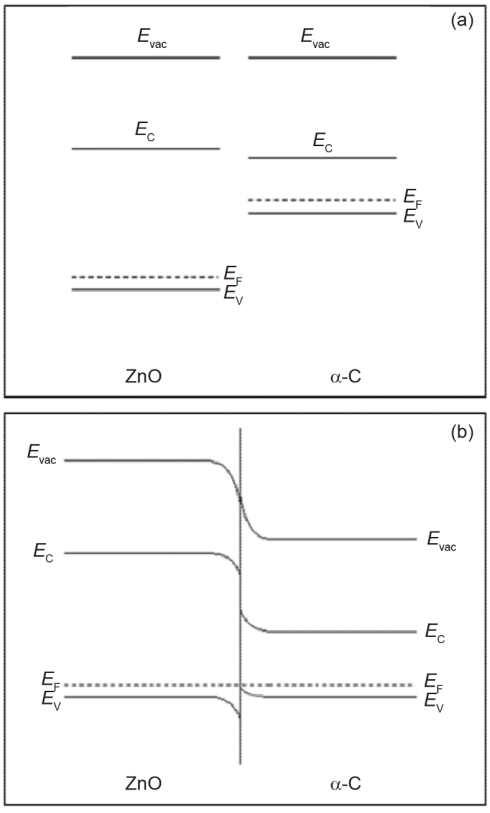

Figure 4 Band structure diagrams. (a) ZnO and carbon, (b) carbon-coated ZnO, adapted with permission from Ref. [67], copyright by IOP Publishing Ltd. (2005), and reproduced for clarity.

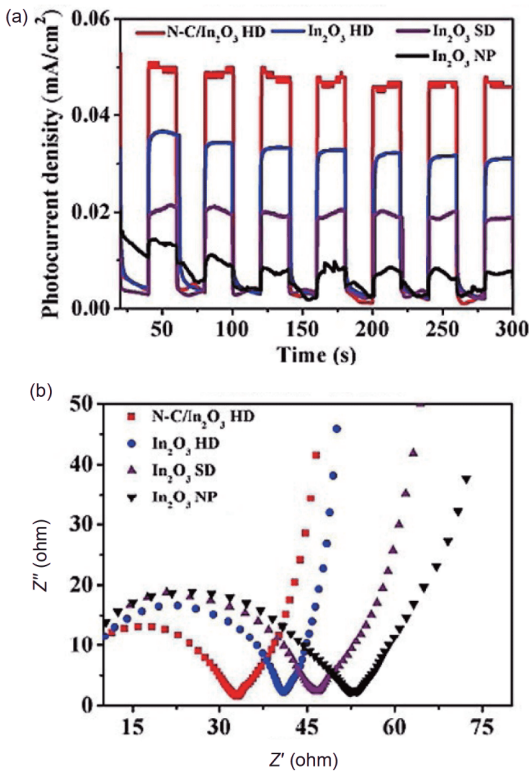

Figure 5 (a) Photocurrent and (b) electrochemical impedance spectroscopy Nyquist plots for N-C/In_2O_3 HD, In_2O_3 HD, In_2O_3 SD and In_2O_3 NP, adapted with permission from Ref. [50], copyright by John Wiley & Sons, Inc. (2019), and reproduced for clarity (color online).

scopy measurements (Figure 5(b)), N-C/In_2O_3 HD featured a smaller semicircle. This further demonstrated the enhanced ability in the electron transfer on N-C/In_2O_3 HD. The enhanced ability in the electron transfer on the N-C/In_2O_3 HD promoted the movement of the electrons from CB of In_2O_3 to N-doped carbon layers, and thus enhanced the separation of photogenerated electron-hole pairs. Theoretical calculations were used to explore the transfer path of the electrons between CB of In_2O_3 and N-doped carbon layers. C–In–Oand N–In–O bonds formed and the highest occupied levels contained the hybrid states of C 2p and N 2p orbitals. Photogenerated electrons transferred from the hybrid states of In_2O_3, including In 5s and O 2p orbitals, to the hybrid states of N-doped carbon layers, including C 2p and N 2p orbitals, through the C–In–O and N–In–O bonds, thus promoting the separation of the photogenerated electron-hole pairs.

Functional groups on the carbon layers were also crucial factors affecting the separation efficiency of photogenerated electron-hole pairs on carbon-coated photocatalysts. Electron-donating groups, such as hydroxyl, phenyl and alkyl groups, can capture the photogenerated holes, whereas electron-withdrawing groups, such as acyl, aldehyde and carboxyl groups, can accept the photogenerated electrons. These are all benefit for electron-hole separation. There are also some functional groups which have been proposed to be the centers for electron-hole recombinations, such as carboxylate and alkoxy groups [68–71]. Liu *et al.* [68] fabricated carbon-coated TiO_2 (C/TiO_{2-x}), and treated C/TiO_{2-x} by acid to fabricate C*/TiO_{2-x}. C/TiO_{2-x} and C*/TiO_{2-x} exhibited similar light absorption but different efficiency in separating the photogenerated electron-hole pairs. C/TiO_{2-x} had alkoxy and carboxylate groups as well as graphite-like carbon, while only graphite-like carbon was observed on the C*/TiO_{2-x}. The graphite-like carbon was conductive in transferring electrons from TiO_2 to carbon layers, thus promoting electron-hole separation (Figure 6). On the other hand, the carboxylate and alkoxy groups were the centers for electron-hole recombinations (Figure 6). Evidently, C/TiO_{2-x} had both charge separation and recombination sites, whereas C*/TiO_{2-x} only contained charge separation sites. As such, more efficient electron-hole separation was achieved on C*/TiO_{2-x}. In addition, it has been suggested that the porous properties of the carbon layers may also play important roles in separating the photogenerated electron-hole pairs, due to the micro-electric fields and multiple bounce of electrons in the porous structures [45–48,69–73].

4 Reactant adsorption

Reactant adsorption on photocatalysts produces active species for triggering photocatalytic reactions [81–84]. Features, including the site, amount, intensity and configuration of reactant adsorption, are key factors to determine the activity, selectivity and stability of photocatalysts [85–91]. For example, dissociative adsorption of CO_2 on photocatalysts favors for the formation of CO, while the interactions of CO_2 with the OH groups on photocatalysts results in bicarbonate species which is an essential intermediate for the formation of CH_3OH [86,89]. But, the adsorption capacities of most of the photocatalysts are poor, mainly due to the smaller surface area and lower conductivity of the photocatalysts. Smaller surface area decreases the amount of active sites for the reactant adsorption [81–84]. Electron transfer has been demonstrated to be the main force to drive the reactant adsorption on photocatalysts [85–91]. The lower conductivity of photocatalysts limits the electron transfer between reactants and photocatalysts, thus suppressing the reactant adsorption. Besides, it should be noting that the reactant adsorption should follow Sabatier principle which shows that only a suitable reactant adsorption, neither too strong nor too weak, can improve the photocatalytic efficiency [81–84].

The carbon layer coating on photocatalysts can enlarge the surface areas of photocatalysts, due to the porous structure of carbon layers [45,59,65,69,92–94]. This improves the reactant adsorption on carbon-coated photocatalysts. Yu *et al.* [45] fabricated carbon-coated Cu_2O photocatalysts (C/Cu_2O).

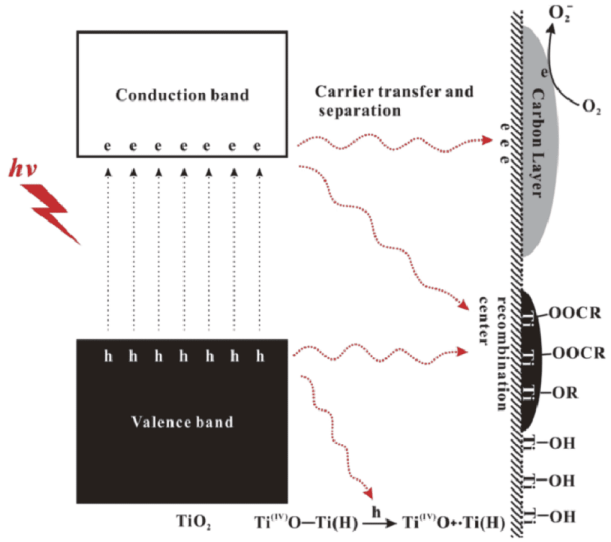

Figure 6 Proposed hole and electron transfer mechanism on carbon-coated TiO_{2-x} upon light irradiation, adapted with permission from Ref. [68], copyright by AIP Publishing LLC. (2018), and reproduced for clarity (color online).

The pure Cu_2O did not have any porous characteristic, with a surface area of only 2.0 m^2 g^{-1}. After coating carbon layers on Cu_2O, a large amount of mesopores were observed, and the surface area was enlarged to 58.93 m^2 g^{-1}. This efficiently improved CO_2 adsorption on C/Cu_2O. The CO_2 adsorption capacity of C/Cu_2O was 13.4 cm^3 g^{-1}, which is about 6 times higher than that on pristine Cu_2O without carbon. In addition to enlarging surface area, the functional groups, *e.g.*, hydroxyl and carboxyl groups, on the carbon layers can also help to improve the reactant adsorption on the carbon-coated photocatalysts. Transfer of the atoms between functional groups on carbon layers and reactants is one of the forces to anchor reactants on photocatalysts [87–91]. For example, proton transfer from carboxyl groups on carbon layers to CO_2 forms a negatively charged HCO_2^- species, thus improving CO_2 adsorption on photocatalysts [87–89]. Non-covalent interactions between functional groups on carbon layers and reactants, including electrostatic and π-π interactions as well as hydrogen bondings, are also important for anchoring reactants on photocatalysts [95–97]. Lee *et al.* [97] prepared a carbon-coated TiO_2 photocatalyst. The adsorption capacity of carbon-coated TiO_2 was about 20 times higher than that of the TiO_2 without carbon, because the carbon layer triggered hydrophobic interactions and oxygenated group mediated electrostatic interactions for improving the reactant adsorption.

The carbon layer coating on photocatalysts is flexible for the electron transfer between photocatalysts and reactants, thus facilitating the reactant adsorption [49,86,98]. Zhang *et al.* [49] coated graphite-like carbon layers with a thickness of about 1 nm on TiO_2 for photocatalytic oxidation of formaldehyde. The photogenerated electrons can be easily transferred into the graphite-like carbon layers. This, on one hand, promoted the separation of photogenerated electron-hole pairs, on the other hand, improved the O_2 adsorption on photocatalysts to form a negatively charged O_2^- species which subsequently triggered formaldehyde oxidation. We previously studied the photocatalytic reduction of CO_2 with H_2O in the presence of pure In_2O_3 (P-In_2O_3) and carbon-coated In_2O_3 (C-In_2O_3). The CO_2 adsorption capacity of C-In_2O_3-based photocatalysts was 2.12 mmol g^{-1}, which was about 2 times higher than that on P-In_2O_3-based photocatalysts (1.03 mmol g^{-1}) (Figure 7(a)). When thickening the carbon layer coating on photocatalysts, the CO_2 adsorption capacity of photocatalysts increased firstly, and then decreased, with the maximum CO_2 adsorption being obtained in the presence of In_2O_3 coated by a 5-nm-thick carbon layer (Figure 7(b)). This was attributed to the higher conductivity of the 5-nm-thick carbon layer [86]. Peng *et al.* [98] found that the N-doped carbon layer with a thickness of about 2 nm coating on CoS_2 can largely promote ion diffusion and electron transfer, thus improving the adsorption capability of photocatalysts for O_2 and organic dyes. This increased the

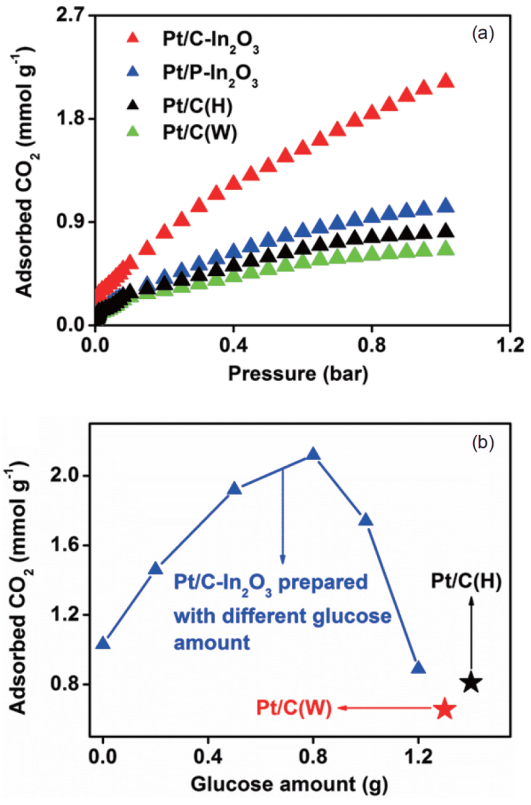

Figure 7 (a) CO_2 adsorption capacities of Pt/C-In_2O_3, Pt/-P-In_2O_3, Pt/C (H), and Pt/C(W). (b) CO_2 adsorption capacity at 1.01 bar as a function of the glucose amount used for preparing carbon-coated In_2O_3. The black and red stars represent the CO_2 adsorption capacities of Pt/C(H) and Pt/C(W), respectively, adapted with permission from Ref. [86], copyright by American Chemical Society (2017), and reproduced for clarity (color online).

efficiency of CoS_2 in photocatalytic oxidation of methylene blue. In addition, it has been proposed that the porous properties of the carbon layers also made some contributions to the electron transfer between photocatalysts and reactants [45,65,82–96].

5 Stability

Stability determines the life time and recyclability of the photocatalysts [4–11]. High-temperature treatments have been widely used in preparing photocatalysts [49,63,92–94]. For example, metal-oxide-based photocatalysts are usually fabricated by using calcinations under the temperatures higher than 500 °C. In the high-temperature treatments, photocatalysts often suffer from the transformation of the crystal phase and aggregation [92–94]. Besides, in the preparation process and photocatalytic reactions, photocatalysts were usually immersed in the corrosive solutions, *e.g.*, acid, alkali and organic reagents. These corrosive solutions have destructive effects on the physicochemical properties of photocatalysts. Coating carbon layers on photocatalysts is a handy but effective strategy to enhance the resistance of photocatalysts to phase transformation, aggregation, acid corrosion and alkali corrosion [37,46,49,59,62,63,75,92–94,97–100]. For example, by coating carbon layers on TiO_2 nanoparticles, Wang *et al.* [37] suppressed the phase transformation and aggregation of TiO_2 nanoparticles, and fabricated anatase TiO_2 nanoparticles with crystal size of about 9 nm. Anatase TiO_2 has a higher photocatalytic activity than rutile TiO_2. However, the transformation from anatase to rutile easily occuring at 600 °C was usually used for preparing TiO_2. When carbon layers were coated on the anatase TiO_2, the energy from high-temperature calcination directly exposes to the carbon layers not to TiO_2. The carbon layer plays as a barrier in suppressing the phase transformation from anatase to rutile, and makes anatase TiO_2 stable even above 600 °C. Besides, the carbon layer coating on anatase TiO_2 can efficiently restrict the crystal aggregation [46].

The carbon layer coating on photocatalysts is a good protector to quench photocorrosion [45,73,83,101–105]. For example, due to the serious photocorrosion, Cu_2O can be easily oxidized into CuO in photocatalytic reactions. Coating carbon layers on Cu_2O not only facilitated the separation of photogenerated electron-hole pairs but also improved the resistance of Cu_2O to photocorrosion, thus enhancing the photocatalytic activity and stability of Cu_2O [45]. Another example, during photocatalytic reactions, photoactive CdS suffers from serious photocorrosion, and can be easily oxidized into CdO with very low photoactivity [101]. Hu *et al.* [101] prepared a carbon-coated CdS (CdS-C-0.5), and studied the stability of the material with Raman spectra. For both pristine CdS and CdS-C-0.5, a peak, due to the longitudinal-optical phonon mode of CdS, was observed at about 295 cm^{-1} on the Raman spectra obtained with a laser power of 300 μW (Figure 8). With increasing the laser power for measuring Raman spectra from 300 to 550 μW, the peak characteristic of CdS at 295 cm^{-1} disappeared for pure CdS, due to the photocorrosion. As for CdS-C-0.5, the characteristic peak of CdS at 295 cm^{-1} was present even at a laser power of 2,500 μW, demonstrating the higher resistance of CdS-C-0.5 to the photocorrosion.

6 Applications of carbon-coated photocatalysts

Due to the improved light absorption, charge separation and transfer, reactant adsorption and stability, carbon-coated photocatalysts showed higher performances in the selective reduction of CO_2 under light irradiation [45,58,78,86]. Yu *et al.* [45] reported that carbon-coated Cu_2O (C/Cu_2O) was efficient for producing CH_4 and C_2H_4 in the photocatalytic reduction of CO_2. The product yield on C/Cu_2O was about two times higher than that on the Cu_2O without carbon (Figure 9). C/Cu_2O exhibited an apparent quantum efficiency of 2.07%, which is higher than those on widely investigated Cu_2O-based photocatalysts like rGO-supported Cu_2O

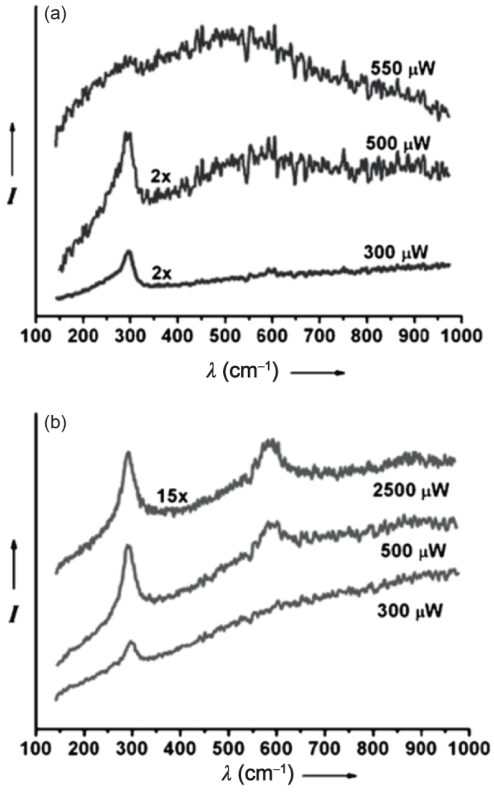

Figure 8 Raman spectra of pristine CdS (a) and CdS-C-0.5 (b) measured at different laser powers, adapted with permission from Ref. [101], copyright by Elsevier (2013), and reproduced for clarity.

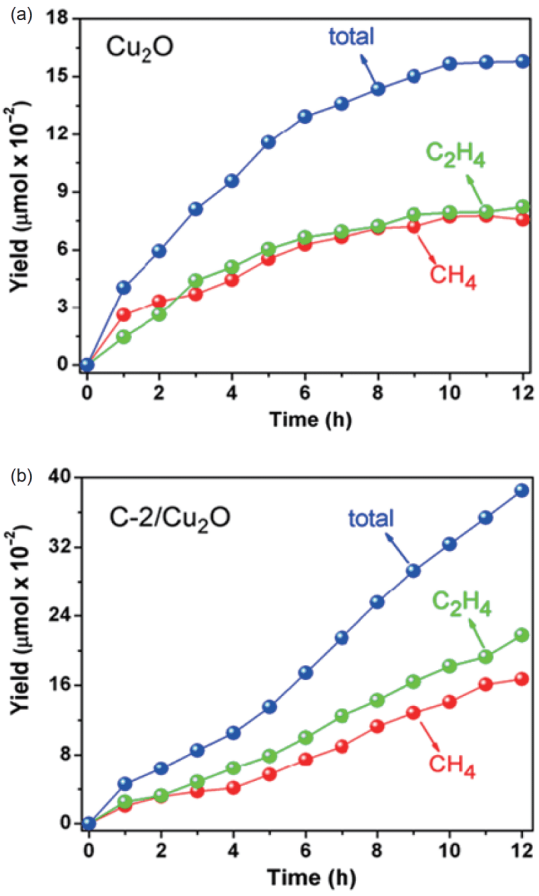

Figure 9 Time-dependent product yield on pure Cu_2O (a) and C/Cu_2O (b), adapted with permission from Ref. [45], copyright by American Chemical Society (2016), and reproduced for clarity (color online).

(0.34%) and Cu_2O/RuO_x (1.6%) photocatalysts. During the photocatalytic reduction, the product yield on pure Cu_2O increased slowly in the first 10 h, and then remained unchanged (Figure 9(a)). But the product yield on C/Cu_2O increased rapidly during the whole photocatalytic reaction (Figure 9(b)). As such, C/Cu_2O had a higher stability. They also explored the stability of pure Cu_2O and C/Cu_2O *via* cycle experiments. After six cycles, the product yield on pure Cu_2O decreased by 46%, while that on C/Cu_2O decreased by only 7%. This further revealed the higher stability of C/Cu_2O. The carbon layer was crucial for the higher activity and stability of C/Cu_2O. Pure Cu_2O without carbon suffered from high electron-hole recombination rates and serious photocorrosion. However, for C/Cu_2O, the carbon layer not only promoted electron-hole separation but also suppressed photocorrosion, thus improving the photocatalytic efficiency.

Kumar *et al.* [58] prepared GO- and rGO-coated ZnO@Fe_3O_4 photocatalysts. They found that CH_3OH was formed during the photocatalytic reduction of CO_2 on ZnO@Fe_3O_4, GO@ZnO@Fe_3O_4 and rGO@ZnO@Fe_3O_4, with the yields in 24 h of 524, 942 and 1,124 μmol $g^{-1}_{cat.}$, respectively. The photogenerated electrons can be easily transferred from ZnO@Fe_3O_4 to GO, leading to more efficient separation of photogenerated electron-hole pairs on GO@ZnO@Fe_3O_4 than that of ZnO@Fe_3O_4. This resulted in the higher CH_3OH yield on GO@ZnO@Fe_3O_4 than that of ZnO@Fe_3O_4. After reducing GO into rGO, the electron mobility and electron-hole separation were further improved, making the CH_3OH production on rGO@ZnO@Fe_3O_4 more efficient than that on GO@ZnO@Fe_3O_4. Similarly, CH_3OH was also produced from photoreducing CO_2 on CuZnO@Fe_3O_4, GO@CuZnO@Fe_3O_4 and rGO@CuZnO@Fe_3O_4. CH_3OH yields in 24 h on CuZnO @Fe_3O_4, GO@CuZnO@Fe_3O_4 and rGO@CuZnO@Fe_3O_4 were 858, 1,749 and 2,656 μmol $g^{-1}_{cat.}$, respectively. The higher electron mobility and more efficient electron-hole separation due to rGO were responsible for the higher CH_3OH yield on rGO@CuZnO@Fe_3O_4 than that of other photocatalysts.

Previously, we found that carbon-coated In_2O_3 (C-In_2O_3) favored for producing CO and CH_4 from the photocatalytic reduction of CO_2 with H_2O (Figure 10) [86]. The CO and CH_4 evolution rates in the presence of C-In_2O_3 were 126.6 and 27.9 μmol h^{-1}, respectively, which were higher than those in the presence of pure In_2O_3 (P-In_2O_3) (CO: 26.7 μmol h^{-1}, CH_4: 4.1 μmol h^{-1}) and commercial TiO_2 (P25) (CO: 12.1 μmol h^{-1}, CH_4: 1.8 μmol h^{-1}) (Figure 10). Besides, the carbon-coated photocatalyst exhibited higher stability. On P-In_2O_3, the band gap between O-2p band and In-4s band was 2.53 eV, indicating that only the high-energy visible and ultraviolet parts of sunlight can be absorbed. On C-In_2O_3, the Fermi level of the carbon layer located at the sites lower than the In-4s band by 0.05 eV, thus lowering the conduction band bottom and narrowing the band gap. This not only improved light absorption but also provided a better match to the potential required for reducing CO_2 with H_2O. C-In_2O_3 had an electronic conductivity of 1.7×10^{-1} S cm^{-1}, which is about 15 times higher than that of P-In_2O_3 (1.1×10^{-2} S cm^{-1}). This resulted in more efficient separation of photogenerated electron-hole pairs on C-In_2O_3. In addition, the carbon layer improved the adsorption of CO_2 on photocatalysts, and promoted the dissociation of H_2O into active hydrogen atoms for reducing CO_2. The narrowing band gap, efficient charge separation, improved CO_2 adsorption and promoted production of active hydrogen atoms due to the carbon layer were the origins for the higher photocatalytic efficiency on carbon-coated materials.

Carbon-coated photocatalysts are also efficient for the photocatalytic splitting of H_2O [65,69,75,77,80,103–105]. Cui *et al.* [80] loaded CdS quantum dots with size of 5 nm on carbon-coated urchin-like Ni_3S_2 to form a noble-metal-free CdS/Ni_3S_2@C composite for the photocatalytic splitting of H_2O (Figure 11). The H_2 production rate on CdS/Ni_3S_2@C (1,164.7 μmol h^{-1}) is about 3.5 times higher than that on the noble-metal-based CdS/Pt photocatalyst (325.2 μmol h^{-1}). In the photocatalytic reaction, CdS quantum dots were re-

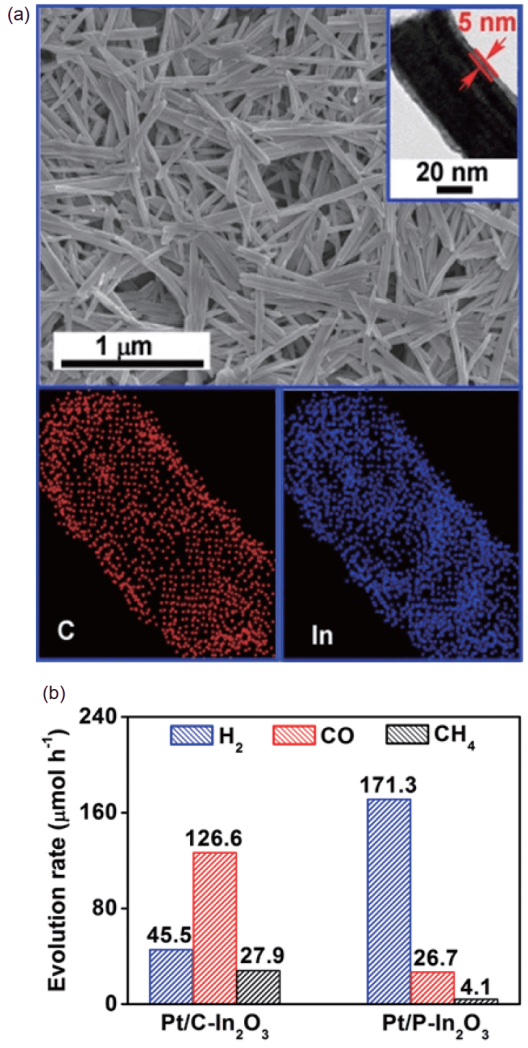

Figure 10 (a) SEM image (upper), TEM image (inset upper) and EDX elemental mappings of C-In_2O_3. (b) H_2, CO and CH_4 evolution rates on Pt/C-In_2O_3 and Pt/P-In_2O_3, adapted with permission from Ref. [86], copyright by American Chemical Society (2017), and reproduced for clarity (color online).

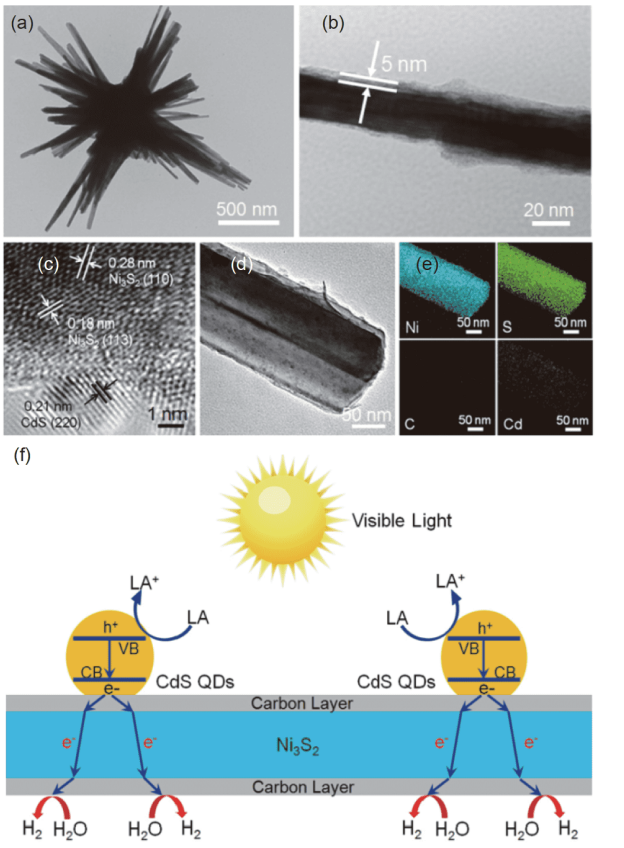

Figure 11 (a, b) TEM images of Ni_3S_2@C. (c) HRTEM image of CdS/Ni_3S_2@C. (d) TEM image of CdS/Ni_3S_2@C. (e) Elemental mapping patterns of Ni, S, C and Cd in CdS/Ni_3S_2@C. (f) Mechanism of the H_2 production from the photocatalytic splitting of H_2O with lactic acid (LA) as a hole scavenger on CdS/Ni_3S_2@C, adapted with permission from Ref. [80], copyright by John Wiley & Sons, Inc. (2018), and reproduced for clarity (color online).

sponsible for absorbing light to form electron-hole pairs, while the role of Ni_3S_2@C was double. On one hand, Ni_3S_2@C played as co-catalysts providing catalytic active sites for splitting H_2O. On the other hand, Ni_3S_2@C promoted electron-hole separation and electron transfer to catalytic active sites. The higher H_2 production rate on CdS/Ni_3S_2@C than that on CdS/Pt implied that the noble-metal-free Ni_3S_2@C is an excellent alternative to Pt. This is helpful for rationally designing and fabricating efficient noble-metal-free photocatalysts. Besides, the carbon-coated photocatalysts can also trigger O_2 production in the photocatalytic splitting of H_2O [65]. By coating carbon layers on TiO_2 nanotubes, Liang *et al.* [65] achieved a highly efficient O_2 evolution from H_2O splitting under the irradiation of light in the full solar spectrum including ultraviolet, visible and infrared lights.

In addition to the photocatalytic reduction of CO_2 and splitting of H_2O, carbon-coated photocatalysts can also enhance the photocatalytic degradation efficiency of pollutants [37,40–42,46–49,68,72,97,101,106,107]. Wang *et al.* [37] applied carbon-coated TiO_2 (C/TiO_2) in photocatalytic degradation of phenol and methylene blue (MB). On C/TiO_2, the time for completely decomposing MB and phenol was 30 and 80 min, respectively. However, only 20% of MB or phenol was decomposed on the TiO_2 without carbon. The enhanced photocatalytic performance was attributed to the more efficient visible light absorption, electron-hole separation, electron transfer and reactant adsorption resulting from the carbon layer coating on TiO_2. Hu *et al.* [101] coated CdS by carbon layers to enhance the photocatalytic degradation efficiency of methyl orange (MO). After irradiation for 40 min, the degradation fraction of MO on pure CdS was 47.8%, whereas that on carbon-coated CdS was as high as 96.6%. The carbon layer coating on CdS improved light absorption, electron-hole separation, reactant adsorption and stability of CdS, thus increasing the photocatalytic efficiency. But, too thick carbon layers coating on CdS may

suppress light absorption and charge transfer, thus decreasing the photocatalytic efficiency.

7 Conclusions and perspective

Research progress in carbon-coated photocatalysts has been summarized in the present review. Coating thin carbon layers on photocatalysts is a handy but efficient strategy to improve light absorption, charge separation and transfer, reactant adsorption and stability of photocatalysts. This makes carbon-coated photocatalysts exhibit enhanced performances for various reactions, *e.g.*, photocatalytic reduction of CO_2, photocatalytic splitting of H_2O and photocatalytic degradation of pollutants.

Despite the important progress, further efforts are still needed for carbon-based photocatalysts. Firstly, innovative preparation methods are needed. At present, hydrothermal method is the widely used preparation method [80,86]. However, there is still a challenge for the hydrothermal method to exactly control the uniformity and thickness of the carbon layers and the carbon-photocatalyst interaction, which are crucial for enhancing photocatalytic efficiency. Recently developed room-temperature-operated plasma technique and three-dimensional printing technique are powerful in fabricating core-shell composite materials [108–110]. These convenient and efficient methods should be emphasized for preparing carbon-coated photocatalysts. Secondly, more materials should be explored for preparing carbon-coated photocatalysts, *e.g.*, zeolites with porous structures [111,112]. The porous structures can result in multiple light reflectance which benefits for light absorption, and provide easy transport and diffusion pathways of electrons and reactants for improving electron-hole separation and reactant adsorption. But, uniformly coating carbon layers on the zeolites without blocking the pores is still a challenge. Thirdly, further more detailed studies on the optical and electrical properties of carbon-coated photocatalysts are highly desired. For example, the action spectrum is efficient for characterizing the ability of photocatalysts in absorbing light [113], while the ultrafast transient absorption spectrum is important for investigating the ability of photocatalysts in the charge separation and transfer [114]. Yet, until now, the action and ultrafast transient absorption spectra of the carbon-coated photocatalysts have not been well explored. Finally, better understanding on the reaction mechanism on the carbon-coated photocatalysts is needed. To determine the reaction mechanism, all of the processes on the photocatalysts, *e.g.*, adsorption, diffusion, transport and desorption of reactants, have to be clarified. This needs not only experimental techniques but also theoretical calculations. However, due to the complexity of the photocatalytic reactions, constructing ideal models matching well with real photocatalytic systems in theoretical calculations is still a challenge.

In conclusion, for carbon-coated photocatalysts, significant improvements have been achieved, but there are still many challenges. However, as a promising strategy to improve the photocatalytic efficiency for solving the energy and environmental problems, it will trigger more studies in the deep-level. Due to the continued and extensive efforts, more efficient carbon-coated photocatalysts will be designed and fabricated for advanced applications.

Acknowledgements This work was supported by the National Natural Science Foundation of China (21922807).

Conflict of interest The authors declare no conflict of interest.

1 Fang Y, Zheng Y, Fang T, Chen Y, Zhu Y, Liang Q, Sheng H, Li Z, Chen C, Wang X. *Sci China Chem*, 2020, 63: 149–181
2 Katal R, Masudy-Panah S, Tanhaei M, Farahani MHDA, Jiangyong H. *Chem Eng J*, 2020, 384: 123384
3 Xiao M, Wang Z, Lyu M, Luo B, Wang S, Liu G, Cheng HM, Wang L. *Adv Mater*, 2019, 31: 1801369
4 Li A, Zhu W, Li C, Wang T, Gong J. *Chem Soc Rev*, 2019, 48: 1874–1907
5 Zhang P, Lou XWD. *Adv Mater*, 2019, 31: 1900281
6 Chen G, Waterhouse GIN, Shi R, Zhao J, Li Z, Wu LZ, Tung CH, Zhang T. *Angew Chem Int Ed*, 2019, 58: 17528–17551
7 Zhou P, Zhang H, Ji H, Ma W, Chen C, Zhao J. *Sci China Chem*, 2020, 63: 354–360
8 Ling X, Xu Y, Wu S, Liu M, Yang P, Qiu C, Zhang G, Zhou H, Su C. *Sci China Chem*, 2020, 63: 386–392
9 Wang J, Zhang J, Peh SB, Liu G, Kundu T, Dong J, Ying Y, Qian Y, Zhao D. *Sci China Chem*, 2020, 63: 192–197
10 Ren F, Luo W, Zou Z. *Sci China Chem*, 2019, 62: 1553–1554
11 Li C, Xu Y, Tu W, Chen G, Xu R. *Green Chem*, 2017, 19: 882–899
12 Schreck M, Niederberger M. *Chem Mater*, 2019, 31: 597–618
13 Li X, Yu J, Jaroniec M, Chen X. *Chem Rev*, 2019, 119: 3962–4179
14 Christoforidis KC, Fornasiero P. *ChemCatChem*, 2019, 11: 368–382
15 Jiang L, Yuan X, Pan Y, Liang J, Zeng G, Wu Z, Wang H. *Appl Catal B-Environ*, 2017, 217: 388–406
16 Dolat D, Quici N, Kusiak-Nejman E, Morawski AW, Puma GL. *Appl Catal B-Environ*, 2012, 115-116: 81–89
17 Zeng L, Zhe F, Wang Y, Zhang Q, Zhao X, Hu X, Wu Y, He Y. *J Colloid Interface Sci*, 2019, 539: 563–574
18 Ong CB, Ng LY, Mohammad AW. *Renew Sustain Energy Rev*, 2018, 81: 536–551
19 Shown I, Samireddi S, Chang YC, Putikam R, Chang PH, Sabbah A, Fu FY, Chen WF, Wu CI, Yu TY, Chung PW, Lin MC, Chen LC, Chen KH. *Nat Commun*, 2018, 9: 169
20 Xu Y, Kraft M, Xu R. *Chem Soc Rev*, 2016, 45: 3039–3052
21 Gawande MB, Fornasiero P, Zbořil R. *ACS Catal*, 2020, 10: 2231–2259
22 Low J, Cheng B, Yu J, Jaroniec M. *Energy Storage Mater*, 2016, 3: 24–35
23 Li X, Yu J, Wageh S, Al-Ghamdi AA, Xie J. *Small*, 2016, 12: 6640–6696
24 Xiang Q, Cheng B, Yu J. *Angew Chem Int Ed*, 2015, 54: 11350–11366
25 Zada A, Muhammad P, Ahmad W, Hussain Z, Ali S, Khan M, Khan Q, Maqbool M. *Adv Funct Mater*, 2020, 30: 1906744
26 Hejazi S, Mohajernia S, Osuagwu B, Zoppellaro G, Andryskova P, Tomanec O, Kment S, Zbořil R, Schmuki P. *Adv Mater*, 2020, 32: 1908505

27 Chai OJH, Liu Z, Chen T, Xie J. *Nanoscale*, 2019, 11: 20437–20448
28 Si Y, Lv Z, Lu L, Liu M, Wen Y, Chen Y, Jin H, Liu J, Song W. *Appl Surf Sci*, 2019, 491: 236–244
29 Dante RC. *Int J Hydrogen Energy*, 2019, 44: 21030–21036
30 Zhao F, Rong Y, Wan J, Hu Z, Peng Z, Wang B. *Catal Today*, 2018, 315: 162–170
31 Li Q, Cui C, Meng H, Yu J. *Chem Asian J*, 2014, 9: 1766–1770
32 Melo MA Jr., Osterloh FE. *ACS Appl Mater Interfaces*, 2018, 10: 27195–27204
33 Fernando KAS, Sahu S, Liu Y, Lewis WK, Guliants EA, Jafariyan A, Wang P, Bunker CE, Sun YP. *ACS Appl Mater Interfaces*, 2015, 7: 8363–8376
34 Zhu L, Liu Y, Peng X, Li Y, Men YL, Liu P, Pan YX. *ACS Appl Mater Interfaces*, 2020, 12: 12892–12900
35 Yang MQ, Xu YJ. *Nanoscale Horiz*, 2016, 1: 185–200
36 Ali S, Razzaq A, In SI. *Catal Today*, 2019, 335: 39–54
37 Wang S, Zhao L, Bai L, Yan J, Jiang Q, Lian J. *J Mater Chem A*, 2014, 2: 7439–7445
38 Ren L, Tong L, Yi X, Zhou W, Wang D, Liu L, Ye J. *Chem Eng J*, 2020, 390: 124558
39 Zhao K, Zhao S, Gao C, Qi J, Yin H, Wei D, Mideksa MF, Wang X, Gao Y, Tang Z, Yu R. *Small*, 2018, 14: 1800762
40 Zhang P, Yang X, Jin Z, Gui J, Tan R, Qiu J. *Appl Catal A-Gen*, 2019, 583: 117145
41 Xu C, Zhu J, Yuan R, Fu X. *Carbon*, 2016, 96: 394–402
42 Xia T, Zhang W, Wang Z, Zhang Y, Song X, Murowchick J, Battaglia V, Liu G, Chen X. *Nano Energy*, 2014, 6: 109–118
43 Chen J, Shi J, Wang X, Cui H, Fu M. *Chin J Catal*, 2013, 34: 621–640
44 Mohamed MA, Wan Salleh WN, Jaafar J, Rosmi MS, Mohd. Hir ZA, Abd Mutalib M, Ismail AF, Tanemura M. *Appl Surf Sci*, 2017, 393: 46–59
45 Yu L, Li G, Zhang X, Ba X, Shi G, Li Y, Wong PK, Yu JC, Yu Y. *ACS Catal*, 2016, 6: 6444–6454
46 Shanmugam S, Gabashvili A, Jacob DS, Yu JC, Gedanken A. *Chem Mater*, 2006, 18: 2275–2282
47 Zhou Y, Wang Y, OuYang X, Liu L, Zhu W. *Semicond Sci Technol*, 2017, 32: 035009
48 Ismail I, Nawawi WI, Nawi MA. *Reac Kinet Mech Cat*, 2015, 114: 323–339
49 Zhang LW, Fu HB, Zhu YF. *Adv Funct Mater*, 2008, 18: 2180–2189
50 Sun L, Li R, Zhan W, Wang F, Zhuang Y, Wang X, Han X. *Chem Eur J*, 2019, 25: 3053–3060
51 Pan Y, Liu X, Zhang W, Liu Z, Zeng G, Shao B, Liang Q, He Q, Yuan X, Huang D, Chen M. *Appl Catal B-Environ*, 2020, 265: 118579
52 Molaei MJ. *Sol Energy*, 2020, 196: 549–566
53 Hu S, Zhu M. *ChemCatChem*, 2019, 11: 6147–6165
54 Kudo A, Miseki Y. *Chem Soc Rev*, 2009, 38: 253–278
55 Chen X, Shen S, Guo L, Mao SS. *Chem Rev*, 2010, 110: 6503–6570
56 Liu X, Iocozzia J, Wang Y, Cui X, Chen Y, Zhao S, Li Z, Lin Z. *Energy Environ Sci*, 2017, 10: 402–434
57 Marschall R, Wang L. *Catal Today*, 2014, 225: 111–135
58 Kumar P, Joshi C, Barras A, Sieber B, Addad A, Boussekey L, Szunerits S, Boukherroub R, Jain SL. *Appl Catal B-Environ*, 2017, 205: 654–665
59 Jiang B, Tang Y, Qu Y, Wang JQ, Xie Y, Tian C, Zhou W, Fu H. *Nanoscale*, 2015, 7: 5035–5045
60 Zhao L, Chen X, Wang X, Zhang Y, Wei W, Sun Y, Antonietti M, Titirici MM. *Adv Mater*, 2010, 22: 3317–3321
61 Zheng X, Hu Y, Li Z, Dong Y, Zhang J, Wen J, Peng H. *J Phys Chem Solids*, 2019, 130: 180–188
62 Sabri NA, Nawi MA, Abu Bakar NHH. *J Environ Chem Eng*, 2018, 6: 898–905
63 Anjum DH, Memon NK, Ismail M, Hedhili MN, Sharif U, Chung SH. *Nanotechnology*, 2016, 27: 365709
64 Zhang Y, Wang L, Ma X, Yang M, Jiang H, Li L, Yuan C, Shi J. *J Colloid Interface Sci*, 2018, 531: 47–55
65 Liang Z, Bai X, Hao P, Guo Y, Xue Y, Tian J, Cui H. *Appl Catal B-Environ*, 2019, 243: 711–720
66 Men YL, You Y, Pan YX, Gao H, Xia Y, Cheng DG, Song J, Cui DX, Wu N, Li Y, Xin S, Goodenough JB. *J Am Chem Soc*, 2018, 140: 13071–13077
67 Liao L, Li JC, Wang DF, Liu C, Liu CS, Fu Q, Fan LX. *Nanotechnology*, 2005, 16: 985–989
68 Liu F, Feng N, Yang L, Wang Q, Xu J, Deng F. *J Phys Chem C*, 2018, 122: 10948–10955
69 Bashiri R, Mohamed NM, Ling LY, Suhaimi NA, Shahid MU, Sufian S, Kait CF, Saheed SM. *Diamond Related Mater*, 2019, 94: 194–202
70 Xu T, Zhang L, Cheng H, Zhu Y. *Appl Catal B-Environ*, 2011, 101: 382–387
71 Wu Y, Ward-Bond J, Li D, Zhang S, Shi J, Jiang Z. *ACS Catal*, 2018, 8: 5664–5674
72 Zhang Y, Zhang Y, Song L, Su Y, Guo Y, Wu L, Zhang T. *RSC Adv*, 2018, 8: 885–894
73 Faraji M, Mohaghegh N. *Surf Coatings Tech*, 2016, 288: 144–150
74 He D, Li Y, Wang I, Wu J, Yang Y, An Q. *Appl Surf Sci*, 2017, 391: 318–325
75 Tong X, Yang P, Wang Y, Qin Y, Guo X. *Nanoscale*, 2014, 6: 6692–6700
76 Zheng X, Wang K, Huang Z, Liu Y, Wen J, Peng H. *J Indust Eng Chem*, 2019, 76: 288–295
77 Sun L, Zhuang Y, Yuan Y, Zhan W, Wang X, Han X, Zhao Y. *Adv Energy Mater*, 2019, 9: 1902839
78 Rambabu Y, Kumar U, Singhal N, Kaushal M, Jaiswal M, Jain SL, Roy SC. *Appl Surf Sci*, 2019, 485: 48–55
79 Cui G, Wang W, Ma M, Zhang M, Xia X, Han F, Shi X, Zhao Y, Dong YB, Tang B. *Chem Commun*, 2013, 49: 6415–6417
80 Cui Y, Pan Y, Qin H, Cong H, Yu S. *Small Methods*, 2018, 2: 1800029
81 Habisreutinger SN, Schmidt-Mende L, Stolarczyk JK. *Angew Chem Int Ed*, 2013, 52: 7372–7408
82 Li K, Peng B, Peng T. *ACS Catal*, 2016, 6: 7485–7527
83 Ding J, Bu Y, Ou M, Yu Y, Zhong Q, Fan M. *Appl Catal B-Environ*, 2017, 202: 314–325
84 Liu L, Zhao C, Miller JT, Li Y. *J Phys Chem C*, 2017, 121: 490–499
85 Pan YX, Sun ZQ, Cong HP, Men YL, Xin S, Song J, Yu SH. *Nano Res*, 2016, 9: 1689–1700
86 Pan YX, You Y, Xin S, Li Y, Fu G, Cui Z, Men YL, Cao FF, Yu SH, Goodenough JB. *J Am Chem Soc*, 2017, 139: 4123–4129
87 Pan Y, Liu C, Ge Q. *Langmuir*, 2008, 24: 12410–12419
88 Pan Y, Liu C, Mei D, Ge Q. *Langmuir*, 2010, 26: 5551–5558
89 Pan Y, Liu C, Ge Q. *J Catal*, 2010, 272: 227–234
90 Baltrusaitis J, Jensen JH, Grassian VH. *J Phys Chem B*, 2006, 110: 12005–12016
91 Wang SG, Cao DB, Li YW, Wang J, Jiao H. *J Phys Chem B*, 2005, 109: 18956–18963
92 Azami MS, Ismail K, Ishak MAM, Zuliahani A, Hamzah SR, Nawawi WI. *J Water Process Eng*, 2020, 35: 101209
93 Scarisoreanu M, Alexandrescu R, Morjan I, Birjega R, Luculescu C, Popovici E, Dutu E, Vasile E, Danciu V, Herlin-Boime N. *Appl Surf Sci*, 2013, 278: 295–300
94 Zhang Z, Zhou Y, Zhang Y, Zhou S, Shi J, Kong J, Zhang S. *Dalton Trans*, 2013, 42: 5004–5012
95 Liu W, Liu Z, Wang G, Sun X, Li Y, Liu J. *Sci China Mater*, 2017, 60: 438–448
96 Datteo M, Liu H, Di Valentin C. *ACS Appl Mater Interfaces*, 2018, 10: 5793–5804
97 Lee S, Kang YI, Ha SJ, Moon JH. *RSC Adv*, 2014, 4: 55371–55376
98 Peng S, Li L, Mhaisalkar SG, Srinivasan M, Ramakrishna S, Yan Q. *ChemSusChem*, 2014, 7: 2212–2220
99 Tsumura T, Kojitani N, Izumi I, Iwashita N, Toyoda M, Inagaki M. *J Mater Chem*, 2002, 12: 1391–1396
100 Kojin F, Mori M, Noda Y, Inagaki M. *Appl Catal B-Environ*, 2008,

78: 202–209
101 Hu Y, Gao X, Yu L, Wang Y, Ning J, Xu S, Lou XWD. *Angew Chem Int Ed*, 2013, 52: 5636–5639
102 Li Y, Chopra N. *Phys Chem Chem Phys*, 2015, 17: 12881–12893
103 Chen S, Yang S, Sun X, He K, Ng YH, Cai X, Zhou W, Fang Y, Zhang S. *Energy Technol*, 2019, 7: 1800846
104 Chen S, Li M, Yang S, Li X, Zhang S. *Appl Surf Sci*, 2019, 492: 571–578
105 Fang LJ, Wang XL, Li YH, Liu PF, Wang YL, Zeng HD, Yang HG. *Appl Catal B-Environ*, 2017, 200: 578–584
106 Mozia S, Toyoda M, Inagaki M, Tryba B, Morawski AW. *J Hazard Mater*, 2007, 140: 369–375
107 Gad-Allah TA, Fujimura K, Kato S, Satokawa S, Kojima T. *J Hazard Mater*, 2008, 154: 572–577
108 Wang W, Wang Z, Wang J, Zhong CJ, Liu CJ. *Adv Sci*, 2017, 4: 1600486
109 Liu C, Ye J, Jiang J, Pan Y. *ChemCatChem*, 2011, 3: 529–541
110 Zhou X, Liu C. *Adv Funct Mater*, 2017, 27: 1701134
111 Dhakshinamoorthy A, Asiri AM, García H. *Angew Chem Int Ed*, 2016, 55: 5414–5445
112 Fechete I, Vedrine JC. *Molecules*, 2015, 20: 5638–5666
113 Lee SK, Mills A, O'Rourke C. *Chem Soc Rev*, 2017, 46: 4877–4894
114 Smith JD, Jamhawi AM, Jasinski JB, Gallou F, Ge J, Advincula R, Liu J, Handa S. *Nat Commun*, 2019, 10: 1837